Article

Journal of
Nanoscience and Nanotechnology
Vol. 14, 3137–3146, 2014
www.aspbs.com/jnn

Vapour Phase Hydrogenolysis of Glycerol Over Nano Ru/SBA-15 Catalysts on the Effect of Preparatory Routes and Metal Precursors

Vanama Pavankumar[1], Chakravartula S. Srikanth[1], Anipindi Nageswara Rao[2], and Komandur V. R. Chary[1,*]

[1] *Catalysis Division, Indian Institute of Chemical Technology, Hyderabad 500007, India*
[2] *Department of Physical and Nuclear Chemistry and Chemical Oceanography, Andhra University, Visakhapatnam 530003, India*

The effect of preparation method and metal precursor of ruthenium employed during the preparation of Ru/SBA-15 catalysts were investigated. The catalytic functionalities are evaluated during the vapour phase hydrogenolysis of glycerol to 1,2-propyleneglycol, 1,3-propylene glycol and ethylene glycol. The catalysts exhibit high conversion/selectivity for 3 wt%Ru (3Ru/SBA-15) catalysts during glycerol hydrogenolysis. CO-chemisorption results suggest that the variation in the dispersion of Ru on SBA-15 support. These catalysts were characterized by XRD, TPR, TEM, BET surface area, pore size distribution and CO-chemisorption measurements. The Ru/SBA-15 catalysts synthesized from micro-emulsion method and polyol method have shown higher catalytic activity than the samples prepared by impregnation method and deposition-precipitation method. The catalytic behavior during glycerol hydrogenolysis is attributed to the formation of nano particles of ruthenium.

Keywords: Ruthenium Catalysts, Glycerol, Dispersion, Hydrogenolysis, SBA-15.

1. INTRODUCTION

Ordered mesoporous silicas have been the focus of much attention since the discovery of the M41 family of materials by the Mobil Corporation in 1992.[1] The use of surfactants as structure directing agents, these silicas are characterized by large surface areas and having narrow pore size distributions.[1] MCM-41 was prepared with the use of cationic surfactants in a basic solution giving hexagonally ordered porous solids with pores sizes of 20 to 30 Å.[2] Using non-ionic tri block copolymers in acidic media, Zhao and co-workers[3] were successful in synthesizing a family of highly ordered mesoporous Santa Barbara Amorphous (SBA) silica with pore sizes up to 300 angstrom. The greater hydrothermal stability and overall mechanical strength offered by the thick pore walls, as well as large surface area and tunable pore size, make SBA-15 an interesting catalyst support.

SBA-15 is a well-ordered hexagonal mesoporous silica structure exhibits uniform cylindrical pores and thick pore walls.[4] It is synthesized with the use of a nonionic tri-block copolymer poly(ethylene oxide)–poly(propylene oxide)–poly(ethylene oxide) PEO20-PPO70-PEO20, commercially known as P123.[4] SBA-15 and typically show surface areas ranging from 600 to 1000 m^2/g depending on reaction temperature and duration.[4] Pore diameters are typically in the range of 40 to 80 Å, without the use of co-solvents or swelling agents such as trimethylbenzene which increases the pore size. As would be expected for silica with cylindrical geometry, the pore size and surface area are inversely proportional to each other, as the pore size decreases, the surface area increases. Pore volumes are typically 0.8 to 1.2 mL/g. However, the most identifiable attribute of SBA-15 is the well ordered, parallel pore structure, consisting of non-intersecting pores, hexagonally oriented, with a pore width to length aspect ratio of 1:1000.[4] SBA-15 is regarded as easy to make bulk nanostructured materials. They posses great potential use in both macroscopic applications and nanotechnology.[5,6] Mesoporous silica nano-materials with large surface area and pore volume can serve as efficient carriers for storage and

*Author to whom correspondence should be addressed.

separation, catalysis, therapeutic agents for drug delivery, nano based targeted cancer therapy.[7,8] The main advantage of SBA-15 materials compared to the supports like Al_2O_3, SiO_2 etc. is its thicker walls, larger pore size and remarkable hydrothermal stability. These properties exhibited by SBA-15 have attracted considerable attention recently for its potential application in catalysis and many catalysts have been prepared by introducing noble metals, and their oxides into the channels of SBA-15.[9]

In the present work, nano structured ruthenium catalysts supported on SBA-15 were prepared and studied for the vapor phase hydrogenolysis of glycerol. Ruthenium nano particles have been employed in numerous applications such as in electronics, optics, magnetic devices as well as in catalysis.[10,11] As the physical and chemical properties depend on the size and shape of the nanoparticles, their applications require non-agglomerated, uniform particles with a controlled mean size and a narrow size distribution. Physical, chemical or electrochemical methods have been used to prepare nanoparticles of uniform size and shape.[12]

The usual synthetic technique for making such nanoparticles involves recently developed chemical methods, including reduction of metal salts in solution-phase,[13] micro-emulsion,[14,15] deposition-precipitation process[16] and impregnation method.[17] Size control of the nanoparticles is achieved through the control of the nucleation and growth by varying the synthesis parameters, including the activity of the reducing reagents, the type and concentration of the precursors, different preparation methods, the nature and amount of surfactants or protective reagents.[13,15] A rigorous control of the different reaction parameters such as temperature, type, amount, and order of addition of reactants, allows control of the size, shape and size distribution of the particles by incorporation of ruthenium in to the mesoporous SBA-15 support. The production of these chemicals from bio-renewable glycerol can be both environmentally and economically attractive routes with Ru-SBA-15.[9,16–18]

In the present investigation we report preparation of nano ruthenium catalysts supported on SBA-15 by using different precursors (chloride and chlorine-free) such as $RuCl_3$ by deposition precipitation method (3Ru(Cl)-DP) and Micro-Emulsion method (3Ru(Cl)-ME) and $Ru(acac)_3$ by Impregnation method (3Ru(A)-Imp) and Polyol method (3Ru(A)-Pol). These catalysts were characterized by XRD, TPR, TEM, BET surface area, pore size distribution and CO-chemisorption measurements. The catalytic performance during hydrogenolysis of glycerol was correlated to the surface structural aspects derived from several characterization techniques. The effects of precursors and preparatory routes have been investigated on the catalytic properties of vapor phase hydrogenolysis of glycerol on 3 wt% nano ruthenium catalysts. In our earlier work we found that 3 wt% ruthenium is the optimum loading exhibiting higher catalytic activity for hydrogenation of nitrobenzene to aniline and also during hydrodechlorination of 1,2,4-trichlorobenzene on SBA-15 and different inorganic supports.[15,17,19] The purpose of this work is to investigate the effect of preparation method and also the precursor employed during the preparation of nano ruthenium on SBA-15 catalysts and further to study its catalytic properties in the vapor phase hydrogenolysis of glycerol.

2. EXPERIMENTAL DETAILS

2.1. Preparation of the SBA-15 and Ru/SBA-15

SBA-15 was prepared by the procedure described by Zhao et al.[20,21] A detailed description of preparation method was given elsewhere.[17] 3 wt% Ru/SBA-15 catalysts are prepared by deposition precipitation (DP) method,[16] micro-emulsion (ME) method[14,15] using $RuCl_3$ as precursor. Impregnation (Imp) method[17] and polyol reduction (Pol) method[13] were employed to prepare the catalysts using Ru $(acac)_3$ precursor. All the catalysts were subsequently dried at 373 K for 16 h and reduced in hydrogen (99.9%) flow at 573 K for 3 h prior to characterization and catalytic activity measurements.

2.1.1. Micro Emulsion

In micro-emulsion method, 0.5 g of cetyltrimethyl ammonium bromide (CTABr) was added to 5 mL of *n*-butanol and 30 mL of cyclohexane until a clear solution is formed. The solution was divided in to two parts. To one part of solution about 5 mL of H_2O and 0.182 g of $RuCl_3$ precursor was added and to the second part about 3–6 drops of hydrazine (a reducing agent) was added for the reduction of ruthenium chloride to metallic Ru. Both the solutions are mixed slowly and required amount of SBA-15 support along with 110 mL of THF (tetrahydrofuran) was added. The mixture was added and stirred for 20 min, and allowed to settle for 10 min. The settled particles were filtered and washed with THF to remove the surfactant completely. Further the filtrate was washed with ethanol and dried in oven at 373 K.

2.1.2. Polyol Method

In this method about 20 mL of ethylene glycol was placed in ice bath at 267 K temperature and 3 g of SBA-15 was added to it. In another container, 0.28 g of $Ru(acac)_3$ was dissolved in 10 ml of ethylene glycol separately. The $Ru(acac)_3$-ethylene glycol solution was added drop wise to 20 ml ethylene glycol in ice bath with constant stirring for 20 min. The final mixture was allowed to settle and the filtrate is washed with ethanol and dried in oven at 373 K.

2.1.3. Deposition Precipitation Method

In this method about 0.182 g of $RuCl_3$ was dissolved in 20 mL of water and 3 g of SBA-15 support was added to the solution and stirred for 30 min and allowed to settle down for 2 h. To the above mixture 0.1 M Na_2CO_3 solution was added with stirring until the pH reaches 10.5.

The mixture was kept stirring for 1 hour and allowed to settle down. The mixture was decanted with distilled water for several times to remove chlorides which was confirmed with $AgNO_3$ test. Subsequently the catalysts are oven dried at 373 K. All the catalysts prepared in the present study are oven dried at 373 K and they are not subjected to any calcination to prevent agglomeration of ruthenium particles. Highly dispersed Ru were also observed in our previous investigations using $RuCl_3$ as precursor for SBA-15 support.[15, 17]

2.2. X-Ray Diffraction Studies

X-ray diffraction patterns were recorded on Rigaku miniflex diffractometer using graphite filtered Cu Kα (K = 0.15406 nm) radiation. Determination of the ruthenium phase was made with the help of JCPDS data files.

2.3. B.E.T Surface Area and Pore Size Distribution

The specific surface area, pore size distribution studies of the pre-reduced catalysts was estimated using N_2 adsorption isotherms at 77 K by the multipoint BET method taking 0.0162 nm^2 as its cross-sectional area using Autosorb 1C (Quantachrome instruments).

2.4. TEM Analysis

The morphological analysis was carried out using transmission electron microscopy (TEM on a JEOL 100 S microscope at high resolution (HR) on a JEOL 2010 microscope). Samples for both TEM analyses were prepared by adding 1 mg of reduced sample to 5 ml of methanol followed by sonication for 10 min. A few drops of suspension were placed on a hollow copper grid coated with a carbon film made in the laboratory.

2.5. CO-Chemisorption

CO chemisorption measurements were carried out on Auto Chem 2910 (Micromeritics, USA) instrument. Prior to adsorption measurements, ca. 100 mg of the sample was reduced in a flow of hydrogen (50 ml/min) at 573 K for 3 h and flushed out subsequently in a pure helium gas flow for an hour at 573 K. The sample was subsequently cooled to ambient temperature in the same He stream. CO uptake was determined by injecting pulses of 9.96% CO balanced helium from a calibrated on-line sampling valve into the helium stream passing over the reduced samples at 573 K. Ruthenium surface area, percentage dispersion and Ru average particle size were calculated assuming the stoichiometric factor (CO/Rus) as 1. Adsorption was deemed to be complete after three successive runs showed similar peak areas.

2.6. Temperature Programmed Reduction (TPR)

Temperature programmed reduction (TPR) experiments were carried out on Auto Chem 2910 (Micromeritics, USA) instrument. In a typical experiment ca. 100 mg of oven dried Ru/SBA-15 sample (dried at 383 K for 12 h) was taken in a U-shaped quartz sample tube. Prior to TPR studies the catalyst sample was pretreated in an inert gas (Argon, 50 ml/min) at 473 K. After pretreatment, the sample was cooled to ambient temperature and the carrier gas consisting of 5% hydrogen balance argon (50 ml/min) was allowed to pass over the sample raising the temperature from ambient to 673 K heating at the rate of 10 K/min. The vapors produced during the reduction were condensed in a cold trap immersed in liquid nitrogen and isopropanol slurry. The hydrogen concentration in the effluent stream was monitored with the TCD and the areas under the peaks were integrated using GRAMS/32 software.

2.7. Catalytic Activity Studies

2.7.1. Hydrogenolysis of Glycerol in Gas Phase

Hydrogenolysis of glycerol ($>$ 99% MERCK Chemicals) was carried out over the catalysts in a vertical downflow glass reactor operating at 548 K and normal atmospheric pressure. In the typical reaction ca. 500 mg of the catalyst, diluted with double the amount of quartz grains was packed between the layers of quartz wool. The upper portion of the reactor was filled with glass beads, which served as pre-heater for the reactants. Prior to the reaction, the catalyst was reduced in a flow of hydrogen (180 mL/min) at 573 K for 3 h. After reduction the reactor was fed with glycerol at 533 K. Hydrogen and an aqueous solution of glycerol were introduced into the reactor through a heated evaporator. The liquid products were collected in a condenser for every 60 minutes were analyzed by Shimadzu-GC 2014 gas chromatograph equipped with a carbowax capillary column with a flame-ionization detector (FID). The products were also identified using HP-5973 quadrupole GC-MSD system using carbowax capillary column.

3. RESULTS AND DISCUSSION

3.1. Characterization Results

3.1.1. Low Angle XRD

The low angle XRD patterns (Fig. 1) of the synthesized materials confirm the typical structure of SBA-15 and show the XRD peaks at 2θ angle of 0.9°, 1.7°, and 1.9°, corresponding to the planes of (100), (110), and (200). The Braggs reflections, confirm the hexagonal symmetry (*P6mm*) of the SBA-15 material.[22] A well-resolved peak at 0.9° and two small peaks at 1.7° and 1.9° also can be seen in Figure 1 for the various 3Ru/SBA-15 catalysts. A shift in the peak position particularly at 1.7° and 1.9° was observed compared to pure SBA-15. This shift indicates the slight modification in the pore structure of the SBA-15 upon Ru doping.[23] The intensity of the peaks at 1.7° and 1.9° for the samples 3Ru(Cl)-DP and 3Ru(A)-Imp decreased considerably due to formation of bulk particles of Ru which are blocking the pores of SBA-15 compared to samples of 3Ru(Cl)-ME and 3Ru(A)-Pol methods.

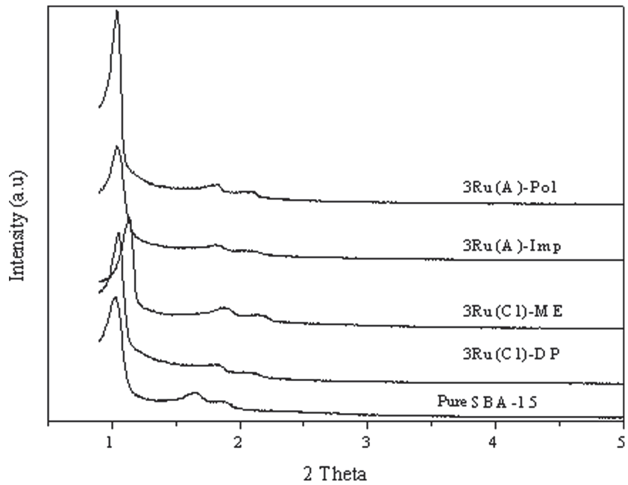

Figure 1. Low angle XRD patterns of pure SBA-15 and 3Ru/SBA-15 catalysts.

3.1.2. Wide Angle XRD

The powder XRD patterns of SBA-15 and various reduced 3Ru/SBA-15 catalysts in the 2θ range of 10–75° are presented in (Fig. 2.) All the samples show a broad peak ranging from $2\theta = 15°–30°$ due to the presence of amorphous silica.[24] It is also observed that catalysts 3Ru(A)-Imp show a broad peak centered at $2\theta = 44°$ due to Ru^{+3}/Ru^0 in crystalline state indicates the formation of Ru^{+3}/Ru^0 phase.[17] The catalysts 3Ru(A)-Pol, 3Ru(Cl)-ME and 3Ru(Cl)-DP did not show any peaks due to Ru^{+3}/Ru^0. Probably due to the presence of highly dispersed state of ruthenium metal particles on SBA-15 having size < 4 nm.

3.1.3. BET Surface Area and Pore Size Distribution Studies

The BET surface area of the pure SBA-15 and 3Ru/SBA-15 catalysts prepared by different preparation methods and precursors are shown in (Table II). These results show that the surface area of pure SBA-15 (650 m^2/g) and decreased further with the introduction of ruthenium on to the support. The considerable decrease in the surface area is due to the deposition of ruthenium particles in the pores of SBA-15 as evidenced from (Figs. 3(A) and (B)) the isotherms and also the average pore diameter of various 3Ru/SBA-15 catalysts. The surface area and pore volume decreased drastically in 3Ru(Cl)-DP and 3Ru(A)-Imp samples compared to 3Ru(A)-Pol and 3Ru(Cl)-ME samples shown in (Table III). This decrease of the surface area can be attributed to formation large ruthenium particles which blocks the pores of SBA-15 support. The sample prepared by DP method have shown Ru particle diameter about 8.1 nm, which is larger than the pore diameter of SBA-15 (7.2 nm) (Table III) and enough to block the pore of SBA-15. However, other catalysts exhibit crystallite size smaller than the pore size of SBA-15 which facilitates the Ru metal to enter in to pores and distribute well inside the walls of the SBA-15. Increase of the crystallite size of Ru in DP method can also be due to the presence of residual Na ions formed during the catalyst preparation using Na_2CO_3.[25] Similar, observations are also made on Cu/SiO_2 catalysts using NaOH as precipitating agent.[26] In impregnation method, due to uneven distribution of the metal precursor solution on the support yields larger crystallites of the metal particles. Low angle XRD and BJH isotherms (Fig. 3) suggest that the hexagonal wall structure of SBA-15 was intact even after the preparation of catalysts by microemulsion method in 3Ru(Cl)-ME. Total pore volume and total pore area of samples were measured by N_2-physisorption are given in (Table II). These findings further suggest that both pore volume and pore area decreases with varying preparation method and Ru precursor employed during the preparation of Ru/SBA-15 catalysts.

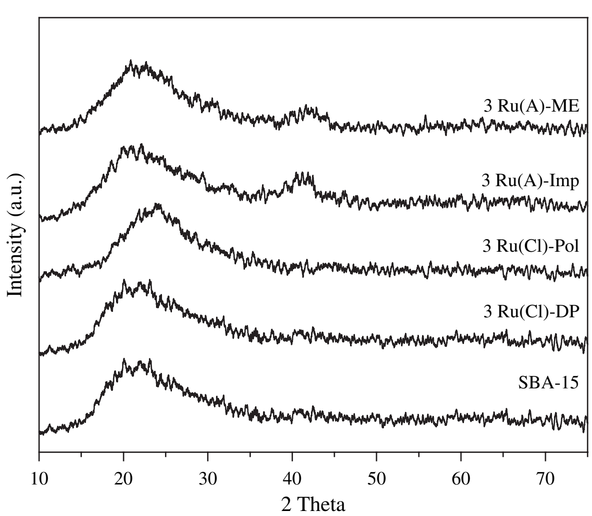

Figure 2. Powder XRD patterns of SBA-15 and various 3Ru/SBA-15 catalysts.

3.1.4. Temperature Programmed Reduction

The H_2-TPR method was used to study the reduction behavior of $RuCl_3$, $Ru(acac)_3$ precursors on SBA-15 and to obtain the information regarding the interaction between the metal and support prepared by different preparation methods and precursors. The H_2-TPR profiles of different Ru/SBA-15 catalysts are presented in (Fig. 4) and the results are reported in (Table I).

The TPR profiles show that the reduction peak appeared with the T_{max} around 400–500 K is attributed to reduction of Ru^{+3}/Ru^0.[17] These peaks are broad due to location of ruthenium ions at different environment.[27] The high temperature peak found in all these catalysts was around 550 K–860 K is attributed to metal-support interactions of particles located in the narrowest pores of SBA-15.[28–30] The catalysts 3Ru(Cl)-DP and 3Ru(A)-Imp show very weak metal-support interaction compared to other catalysts 3Ru(Cl)-ME and 3Ru(A)-Pol. This phenomenon is

Table I. TPR data of various Ru/SBA-15 catalysts.

Catalyst (3 wt%)	T^1_{max}	H_2 uptake (μmol)	T^2_{max}	H_2 uptake (μmol)	T^3_{max}	H_2 uptake (μmol)	T^4_{max}	H_2 uptake (μmol)	Total H_2 uptake (μmol)
Ru(Cl)-DP	433	16	–	–	656.0	113.0	–		132.0
Ru(Cl)-ME	520	217	–	–	753.0	263.0	–		480.0
Ru(A)-Imp	511	290	546	311.0	–	–	–		601.0
Ru(A)-Pol	–	–	565	166.9	–	–	869.0	314.0	480.0

Note: T^1_{max} = 1st peak; T^2_{max} = 2nd peak; T^3_{max} = 3rd peak; T^4_{max} = 4th peak.

observed due to formation of nano particles for the samples prepared through these methods of catalysts preparation.

3.1.5. CO-Chemisorption

The physical properties of 3Ru/SBA-15 catalysts such as dispersion, metal surface area and average particle size obtained from CO-chemisorption are given in (Table III). The dispersion of Ru was calculated from CO-chemisorption using the following equation assuming the cubic particle with five sides exposed to the gas plane,

$$\%\text{Dispersion} = (\text{Number of suface ruthenium atoms} \times 100) / \text{Total number of ruthenium atoms}$$

$$\text{Average particle size} = 6000/(\text{Ru metal surface area per gram of Ru} \times \text{Ru density})$$

The ruthenium metal areas were determined using the equation SCO = nmsXmns^{-1}, where SCO is the total metallic surface area, nmS is the CO consumption and Xm is chemisorption stoichiometry at monolayer coverage, and ns^{-1} is the number of ruthenium atoms per unit surface area. These results strongly influence the dispersion of ruthenium metal in Ru/SBA-15 prepared by various methods described above and the precursors used. The catalysts 3Ru(A)-Pol and 3Ru(Cl)-ME catalysts exhibit higher dispersion and possesses smaller particle size than the catalysts prepared by 3Ru(Cl)-DP and 3Ru(A)-Imp methods. The low CO-uptake in DP and Imp method is probably due to the formation of larger particles with uneven distribution of Ru metal particles on the support.

The ruthenium dispersion on SBA-15 support for different preparation methods and precursors vary from 6% to 25%. The high dispersion of ruthenium in the samples prepared by 3Ru(A)-Pol and 3Ru(Cl)-ME catalysts is due to strong metal support interaction between ruthenium and SBA-15 and growth of nano particles in these catalysts. The low dispersion of Ru in 3Ru(Cl)-DP catalyst is due to formation of larger crystallites of ruthenium in deposition precipitation method. Huang et al.[26] reported that bigger crystallite size of Cu was observed in Cu/SiO_2 catalysts prepared by DP method using NaOH as precipitating agent. The reason for increase in crystallite size is explained on the basis of pH of the solution. The initial pH of the mixture was assumed to be pH 3, with positively charged Si surface and its inability to bind the Cu^{2+}

Table II. BET surface area and Pore size distribution data of SBA-15 and various Ru/SBA-15 catalysts.

Ru (3 wt%)	BET surface area (m^2/g)	Pore diameter (nm)	Pore volume (cc/g)
SBA-15	650	7.5	1.24
Ru(Cl)-DP	250	6.0	1.01
Ru(Cl)-ME	470	6.8	1.20
Ru(A)-Imp	360	5.8	1.12
Ru(A)-Pol	480	7.0	1.15

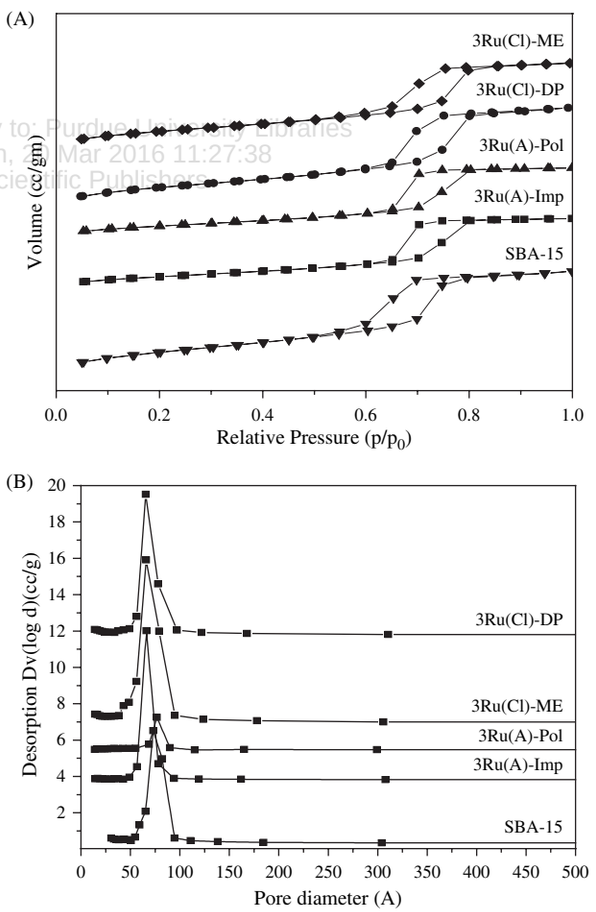

Figure 3. (A) Nitrogen adsorption–desorption isotherms and pore size distributions (B) BJH pore size distribution of SBA-15 and 3Ru/SBA-15 catalysts.

Table III. CO-chemisorption of various 3Ru/SBA-15 catalysts.

Catalyst (3 wt%)	CO uptake (μmol/g)	(%) Dispersion	Metal area $(m^2/g)_{catalyst}$	Particle size^a (nm)	Particle size^b (nm)
SBA-15	–	–	–	–	–
Ru(Cl)-DP	17	6.0	29.3	8.1	7.5
Ru(Cl)-ME	71	24.1	113.5	2.3	2.1
Ru(A)-Imp	47	16.1	78.4	3.2	3.4
Ru(A)-Pol	67	22.7	110.6	2.8	3.2

Notes: *a* = determined from CO uptake values; *b* = determined from TEM analysis.

particles. Later when the pH of the solution is increased beyond 7 by adding basic solution of NaOH, agglomeration of $Cu(OH)_2$ nanoparticles takes place leading to larger crystallite size. However, in the present work the Ru/SBA-15 catalysts exhibited higher stability towards hydrogenolysis of glycerol compared to the catalysts prepared from homogeneous precipitation using urea evaporation. Same explanation can be interpreted here for the increase in crystallite size of Ru in the 3Ru(Cl)-DP catalyst in the present study. Hence, Na_2CO_3 precipitation was employed for the preparation of the catalysts in DP method.[26]

The other factor is, DP method catalyst is not suitable for the supports like SBA-15 having iso-electric point less than 5. It is evident from Table III that the irreversible CO uptake values are more in the catalysts prepared by Pol-method, ME-method, Imp-method and less for DP-method catalyst. The CO-chemisorption results are well in agreement with the findings from the results of H_2-TPR, BET-SA and Pore size distribution studies.

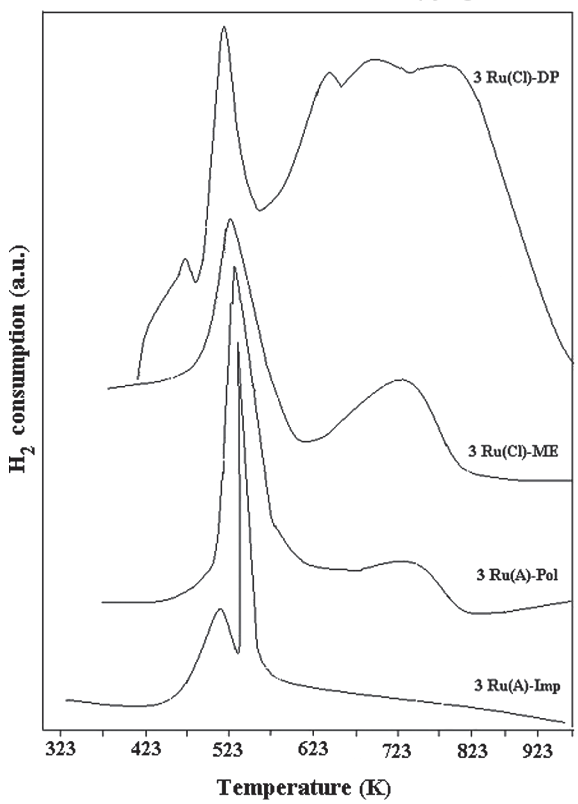

Figure 4. H_2 TPR profiles of various 3Ru/SBA-15 catalysts.

3.1.6. Transmission Electron Microscopy (TEM)

TEM is a powerful technique to investigate the particle size and distribution of metal particles. The TEM images of various 3Ru/SBA-15 samples are presented in (Fig. 5). The catalysts 3Ru(A)-Imp, 3Ru(A)-Pol, and 3Ru(Cl)-ME show the presence of metal particles inside the channels of SBA-15 and pore structure of the SBA-15 was clearly observed, indicating that Ru is present in highly dispersed form. However, in case of 3Ru(Cl)-DP, ruthenium is present all over the catalyst suggesting that Ru is present outside the channels due to its larger crystallite size, which obstruct the SBA-15 channels. The TEM results are also in agreement with the BET surface area and pore-size distribution. The crystallite size of Ru estimated from TEM is well in agreement with the crystallite size measurement from CO-chemisorption experiments.

3.2. Catalytic Activity

3.2.1. Hydrogenolysis of Glycerol to Propane Diols

The hydrogenolysis of glycerol by various Ru/SBA-15 catalysts is shown in (Fig. 6). The effect of catalysts preparation method and also the kind of precursor used during preparation were examined on the hydrogenolysis functionalities. The results show that the 3Ru(A)-Pol exhibit superior activity when compared to all other catalyst employed in the present study. The high activity of the catalysts can be attributed to the smaller crystallite size of Ru on the SBA-15 and also the acetylacetonate precursor used in the study. Hydrogenolysis of glycerol gives rise to various products including 1,2-propylene glycol ethylene glycol, 1,3-propylene glycol, hydroxyacetone, 1-propanol along

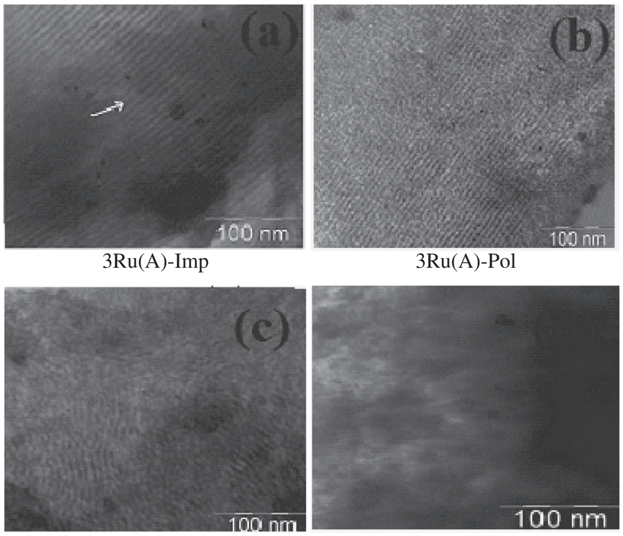

3Ru(A)-Imp 3Ru(A)-Pol
3Ru(Cl)-ME 3Ru(Cl)-DP

Figure 5. TEM images of various 3Ru/SBA-15 catalysts.

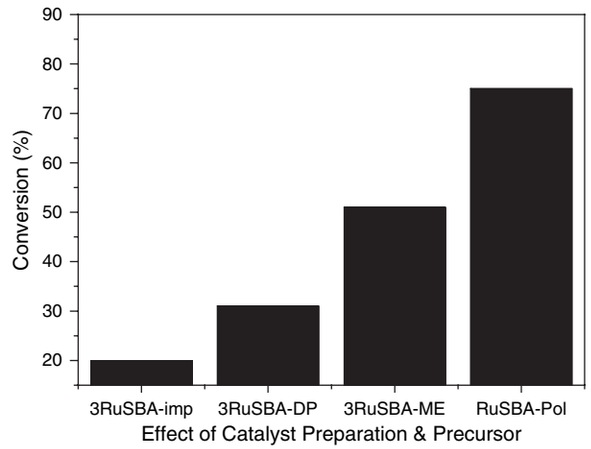

Figure 6. Effect of preparation method and precursor on conversion of Glycerol.

with other major by-products represented as others in the present study. The reaction also produces some degradation products which constitutes of ethanol, methanol, ethane, methane and are represented as others in the present study. The selectivities of various reaction products on different catalysts for glycerol hydrogenolysis are shown in (Fig. 7). Liu et al.[31] prepared various cobalt nanostructures such as cobalt nests, nanoflowers and nanowires and used them as hydrogenolysis catalysts of glycerol and obtained good selectivities.[31, 32] Tomishige et al.[33] proposed the reaction mechanism for glycerol hydrogenolysis in liquid phase on various Ru catalysts[33, 34] with good conversions obtained and selectivities of corresponding desired products.

3.2.2. *Effect of Ru Loading on the Conversion and Selectivity*

To verify the effect of Ru loading on the catalytic activity the samples containing Ru 1, 3 and 5 wt% Ru(A) were

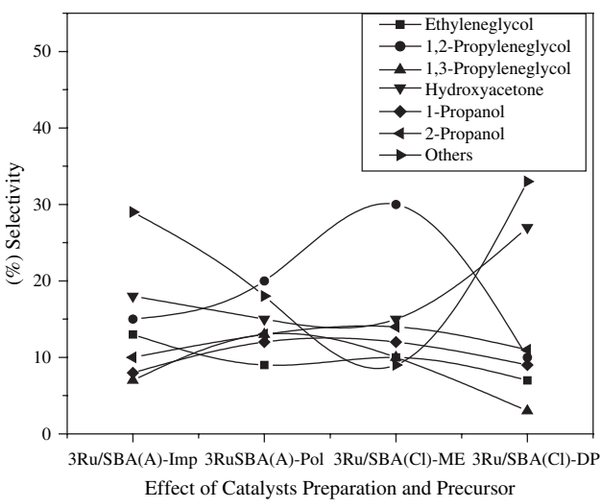

Figure 7. Selectivity of glycerol to propane diols over 3Ru/SBA-15 catalysts.

Table IV. Effect of ruthenium loading on conversion and selectivity for hydrogenolysis of glycerol.

		Selectivity (%)						
Ru wt (%)	Conversion (%)	1,2 PG	1,3 PG	HA	1P	2P	EG	Others
1Ru(A)-Pol	30	11	5	35	10	6	5	28
3Ru(A)-Pol	75	20	13	15	12	13	9	18
5Ru(A)-Pol	55	14	8	6	9	5	6	42

Notes: 1,2 PG = 1, 2 propylene glycol; 1,3 PG = 1, 3 propylene glycol; HA = hydroxyacetone; 1P = 1-propanol; 2P = 2-propanol; EG = ethylene glycol; Reaction conditions Catalyst: Catalyst weight: 0.5 g, Temperature: 533 K, Feed rate: 1 ml/hr, H_2 Flowrate: 240 ml/min, Glycerol Conc: 40 wt%.

prepared by polyol method and the activity results are presented in Table IV. These results show that the conversion of glycerol increases up to 3 wt% and decrease at higher loadings. The result also reveals that at lower loadings the selectivity is high towards hydroxyacetone (HA) and at higher loadings the selectivity is high towards degradation products (others). At 3 wt% Ru loading, the selectivity is high towards propylene glycol isomers. Hence, 3 wt% ruthenium is considered as optimum metal loading for the present study. The optimum loading might change for different preparation methods and different precursors but for the purpose of comparison 3 wt% Ru loading is selected for glycerol hydrogenolysis and studied in detail to understand various reaction parameters on catalytic functionalities.

3.2.3. *Effect of Reaction Temperature*

Figure 8 shows the influence of reaction temperature on the hydrogenolysis of glycerol examined for all the catalysts. All the catalysts show a slight increase in the conversions of glycerol when the temperature of the reaction

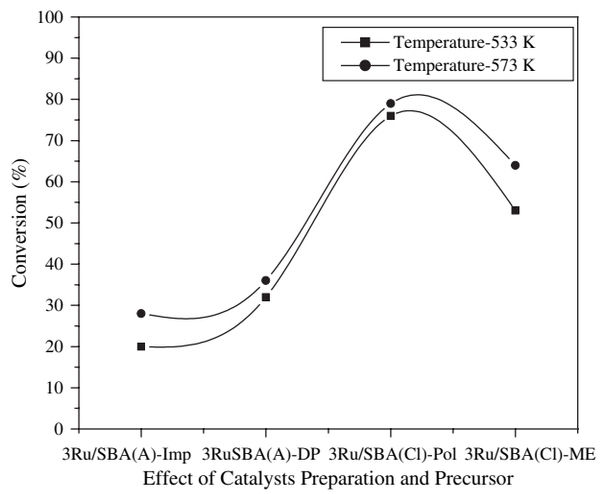

Figure 8. Effect of temperature on hydrogenolysis of glycerol to propane diols reaction conditions: catalyst weight: 0.5 g 3Ru(A)-Pol, temperature varied: 533 K and 573 K, feed rate: 1 ml/hr, H_2 flow rate: 240 ml/min, glycerol concentration: 40 wt%.

increased from 533 K to 573 K. The glycerol conversion gradually increased from 76% to 80% as the temperature of the reaction increased from 533 K to 573 K. The selectivity of various reactions products for 3Ru(A)-Pol method are 1,2-PG (20%), 1,3-PG (13%), EG (9%), 1P (12%), 2P (13%) and HA (15%). Increase in reaction temperature to 573 K increases the conversions from 76 to 80%. However decreases the selectivity towards the desired reactions products 1,2-PG (12%), 1,3-PG (8%), EG (7%), 1-P (8%), 2-P (9%) and HA (25%). The results show that an increase in degradation products was noticed from 18 to 32%. The reason for the increase in degradation products is at higher temperatures is probably due to further hydrogenolysis of propanediols to yield lower alcohols.[29,31]

3.2.4. Effect of H_2-Flow Rate

The influence of H_2-flowrate on hydrogenolysis was studied by carrying out the reaction under various of H_2 flow rates ranging from 180 to 240 mL/min. (Fig. 9) shows the effect of H_2 flow rate on conversion and selectivity during glycerol hydrogenolysis. The glycerol conversion gradually increased with the increase in H_2-flow rate. The selectivity towards desired products 1,2-PG (16%), 1,3-PG (10%), EG (6%), 1-P (9%), 2-P (7%) and HA (30%) decreased with the decrease of H_2-flowrate at 180 mL/min. The high conversion of glycerol with increase in H_2-flowrate is due to the availability of number of Ru sites for the hydrogenolysis of glycerol during the reaction.

3.2.5. Effect of Glycerol Concentration

The Influence of glycerol concentration in water during glycerol hydrogenolysis were investigated. The results presented in (Fig. 10) clearly show that the considerable decline in glycerol conversion is noticed with increase in glycerol concentration in the feed. Similar results of increase in glycerol conversion at low glycerol concentration are reported.[35–37] The selectivity obtained towards high glycerol concentration (60 wt%) were 1,2-PD (8%), 1,3-PD (3%), EG (4%), 1-P (5%), 2-P (4%) and HA (23%) at high glycerol concentration. The low conversion and selectivity at high glycerol concentration is expected to limited availability of active Ru sites on the catalysts.

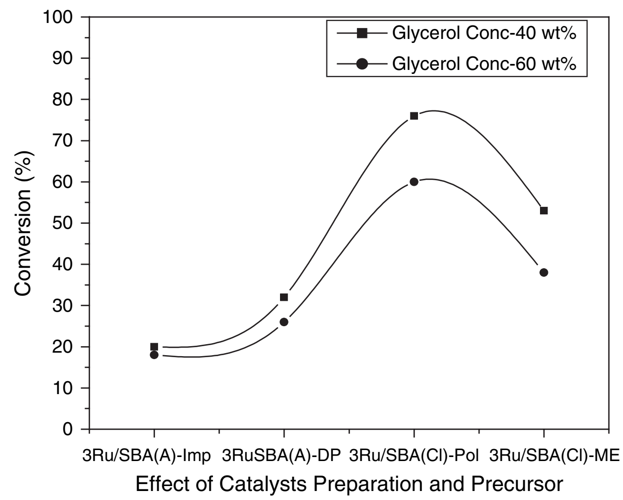

Figure 10. Effect of Glycerol concentration on hydrogenolysis of glycerol to propane diols. Reaction conditions: catalyst weight: 0.5 g, 3Ru(A)-Pol, temperature: 533 K, feed rate: 1 ml/hr, H_2 flow rate: 240 ml/min; glycerol concentration: 40 wt% and 60 wt%.

3.2.6. Effect of Feed Flow Rate

The influences of feed flow rate on glycerol hydrogenolysis was examined and the results are presented in (Fig. 11). It shows that a decrease in glycerol conversion was noticed

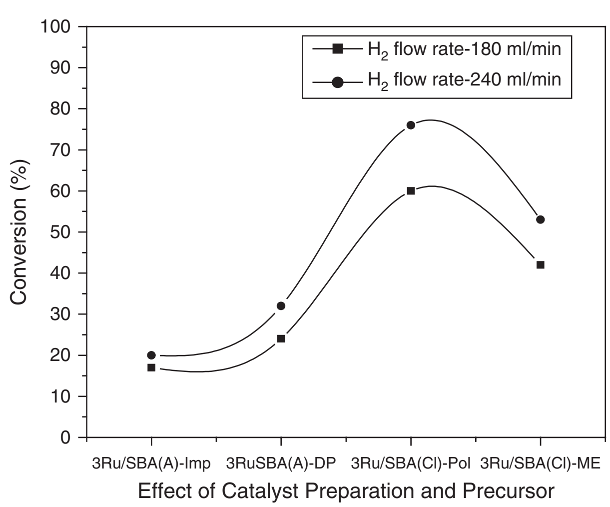

Figure 9. Effect of H_2-flow rate on hydrogenolysis of glycerol to propane diols reaction conditions: catalyst weight: 0.5 g 3Ru(A)-Pol, temperature: 533 K, feed rate: 1 ml/hr, H_2 flow rate: 240 ml/min and 180 ml/min, glycerol concentration: 40 wt%.

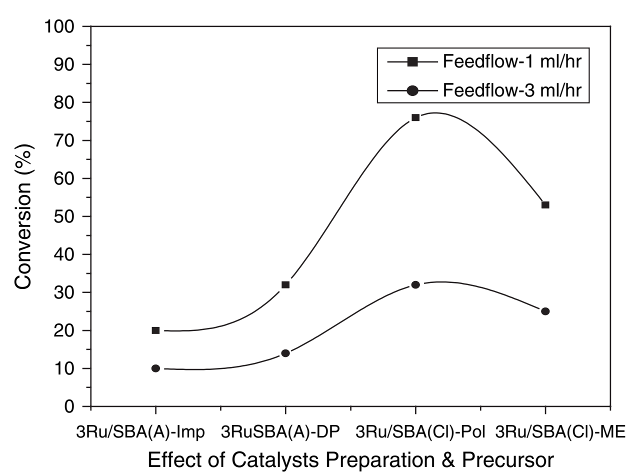

Figure 11. Effect of feed flow rate on hydrogenolysis of glycerol to propane diols reaction conditions: catalyst weight: 0.5 g 3Ru(A)-Pol: temperature: 533 K, feed rate: 1 ml/hr and 3 ml/hr, H_2 flow rate: 240 ml/min; glycerol concentration: 40 wt%.

with increase of glycerol flow rate from 1 mL/hr to 3 mL/hr. It is known that glycerol conversion is higher at low glycerol flow rate of 1 mL/hr. The selectivities obtained at glycerol flowrate of 3 mL/hr is 1,2-PG (13%), 1,3-PG (6%), EG (5%), 1-P (6%), 2-P (7%) and HA (31%). The low conversion and selectivities at high glycerol feed flow rate is as expected, since the available number of Ru sites remain unchanged.

3.2.7. Dependence of Catalytic Properties on Reaction Time

The time on stream studies on the 3% Ru/SBA-15 catalysts were investigated to understand the stability of catalysts during glycerol hydrogenation and the results are shown in (Fig. 12). These results show that 3Ru(A)-Pol exhibit higher conversion (76%) compared to other catalysts. The catalysts prepared by ME method 3Ru(Cl)-ME exhibit lower conversion than 3Ru(A)-Pol but exhibit good selectivity towards propylene glycols. The results suggest that 3Ru(Cl)-DP and 3Ru(A)-Imp exhibit lower conversions, due to their large crystallite sizes compared to 3Ru(A)-Pol and 3Ru(Cl)-ME catalysts. Although the initial activity is higher for 3Ru(A)-Pol catalyst, the activity abruptly dropped from 75% to 10% within 3 hours of operation. 3Ru(A)-ME catalyst exhibit initial activity of 51% and decreases with time compared to other catalysts, suggesting that it was a best catalyst for the glycerol hydrogenolysis of our present investigation. The reasons for faster deactivation of catalysts prepared by polyol method is probably due to carbon deposition and also due to the organic precursor (acetyl acetonate) employed during the preparation. The catalytic activity is correlated with the crystallite size of Ru on different catalysts. The 3Ru(Cl)-DP method and 3Ru(A)-Imp method catalysts were attributed to the decrease in the number of active sites of ruthenium on SBA-15 due to agglomeration as evident from XRD, TEM and CO-chemisorption results.

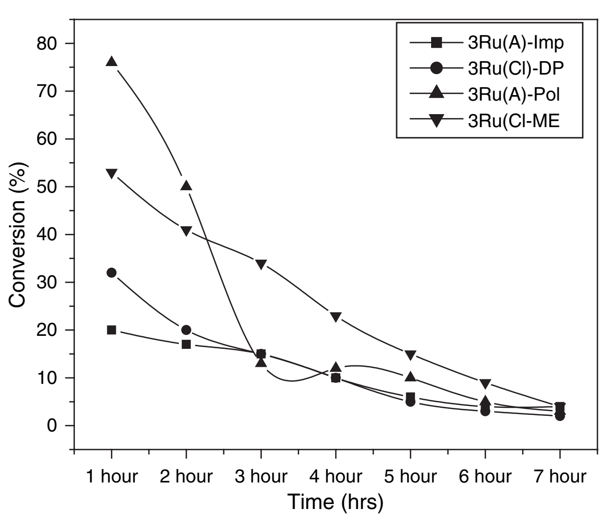

Figure 12. Hydrogenolysis of glycerol to propane diols over 3Ru/SBA-15 catalysts reaction conditions: weight of the catalyst = 500 mg; reaction temperature = 533 K; H_2 flow rate = 240 ml/min, feed flow rate = 1 ml/hr, glycerol concentration = 40 wt%.

3.2.8. Effect of Preparation Method and Precursor on the Catalytic Activity

The catalytic activity of the Ru/SBA-15 catalysts for the glycerol hydrogenolysis varied with the preparation method and precursor used. The catalysts prepared from Chloride precursors 3Ru(Cl)-ME exhibited better activity and stability over a period of time than 3Ru(Cl)-DP method. The high activity in ME catalysts can be attributed to its nano sized ruthenium particles developed during its preparation. Whereas in DP method large crystallites of Ru obtained due to agglomeration of Ru particles during precipitation with Na_2CO_3 and also suffers from residual Na remained during the catalyst preparation.[25] EDAX-analysis suggest that the concentration is present at $< 0.08\%$. The chlorides in 3Ru(Cl)-DP are completely washed during the preparation. Even though 3Ru(Cl)-DP catalysts exhibit low activity exhibited decent stability. The catalysts prepared from $Ru(acac)_3$ precursor 3Ru(A)-Pol showed high initial activity and degraded completely with in 3 h of operation. The reasons for sudden decrease of catalytic activity for polyol catalyst is unclear and require further investigation. 3Ru(A)-Imp also showed poor activity than all other catalysts. The results suggest that the $RuCl_3$ is found to be a better precursor and micro emulsion method is a better method for the preparation of nano sized ruthenium particles.

4. CONCLUSIONS

Highly dispersed ruthenium catalysts confined to pores of SBA-15 support were synthesized by the impregnation, micro emulsion and polyol methods using $RuCl_3$ and $Ru(acac)_3$ precursors. In deposition precipitation method, the use of Na_2CO_3 as a precipitating agent causes agglomeration of ruthenium particles leading to bigger crystallite sizes deposited outside the pores of SBA-15. The confinement of Ru in to the pores of SBA-15 was determined by the BET surface area, pores size distribution results are well in agreement with the CO-chemisorption and TEM results. The ruthenium supported SBA-15 catalysts of different preparation methods and precursors exhibit good catalytic activity for the hydrogenolysis of glycerol to propane diols. Moreover, high selectivity towards the formation of 1,2-Propylene glycol, Ethylene glycol, 1,3-Propylene glycol, 1-Propanol, 2-Propanol and Hydroxyacetone makes Ru more promising for hydrogenolysis of glycerol reaction. The catalysts prepared by polyol method exhibit high initial activity and decreases rapidly suggesting that Ru $(acac)_3$ is not a suitable precursor for the preparation of catalysts. The catalyst prepared from $RuCl_3$ precursor with micro emulsion method exhibits higher activity with good stability compared to other preparation

routes due to the formation of nano-ruthenium supported on SBA-15.

Acknowledgments: The authors Vanama Pavankumar and Chakravartula S. Srikanth thank CSIR, New Delhi for the award of Senior Research Fellowships.

References and Notes

1. K. S. W. Sing, D. H. Everett, R. A. W. Haul, L. Moscou, R. A. Pierotti, J. Rouquerol, and T. Siemieniewska, *Pure and Appl. Chem.* 57, 603 (**1985**).
2. C. T. Kresge, M. E. Leonowicz, W. J. Roth, J. C. Vartuli, and J. S. Beck, *Nature.* 359 710 (**1992**).
3. P. Yang, D. Zhao, D. I. Margolese, B. F. Chmelka, and G. D. Stucky, *Nature* 396 152 (**1998**).
4. F. Jiao and P. G. Bruce, *Angew. Chem. Int. Ed.* 43, 5958 (**2004**).
5. K. Ariga, A. Vinu, Y. Yamauchi, Q. Ji, and J. P. Hill, *Bull. Chem. Soc. Jpn.* 85, 1 (**2012**).
6. Z. Li, J. C. Barnes, A. Bosoy, J. F. Stoddart, and J. I. Zink, *Chem. Soc. Rev.* 41, 2590 (**2012**).
7. W. Xuan, C. Zhu, Y. Liu, and Y. Cui, *Chem. Soc. Rev.* 41, 1677 (**2012**).
8. F. Tang, L. Li, and D. Chen, *Adv. Mater.* 24, 1504 (**2012**).
9. J. Guo, R. Ruan, and Y. Zhang, *Ind. Eng. Chem. Res.* 51, 6599 (**2012**).
10. Y. Chen, K. Y. Liew, and J. Li, *Mater. Lett.* 62, 1018 (**2008**).
11. K. R. Brown, D. G. Walter, and M. J. Natan, *Chem. Mater.* 12, 306 (**2000**).
12. D. H. Chen, J. J. Yeh, and T. C. Hung, *J. Colloid Interface Sci.* 215, 159 (**1999**).
13. S. Devarajan, P. Bera, and S. Sampath, *J. Colloid Interface Sci.* 290, 117 (**2005**).
14. A. Venugopal and M. S. Scurrell, *Appl. Catal., A: General* 245, 137 (**2003**).
15. K. V. R. Chary, Ch. S. Srikanth, and V. V. Rao *Catal. Commun.* 10, 459 (**2009**).
16. X. Zhang and K. Y. Chan *Chem. Mater.* 15, 451 (**2003**).
17. K. V. R. Chary and Ch. S. Srikanth, *Catal. Lett.* 128, 164 (**2009**).
18. D. R-Luyanda, J. F-Cruz, P. J. M-Pérez, L. G. E-Gómez, F. Shi, P. M. Voyles, and N. C-Martínez, *Topics Catal.* 55, 148 (**2012**).
19. Ch. S. Srikanth, V. Pavan Kumar, B. Viswanadham, and K. V. R. Chary, *Catal. Commun.* 13, 69 (**2011**).
20. D. Y. Zhao, J. Feng, Q. Huo, N. Melosh, G. H. Fredrickson, B. F. Chmelka, and G. D. Stucky, *Science,* 279, 548 (**1998**).
21. D. Y. Zhao, Q. Huo, J. Feng, B. F. Chmelka, and G. D. Stucky, *J. Am. Chem. Soc.* 120 6024 (**1998**).
22. V. Mazzieri, N. Figoli, F. Pascual, and P. L'Argentiere, *Catal. Lett*. 102, 79 (**2005**).
23. Y. Chen, J. Han, and H. Zhang, *Appl. Surf. Sci.* 253, 9400 (**2007**).
24. J. Barbier, Jr, F. Delanoe, F. Jabouille, D. Duprez, and J. B. G. Isnard *J. Catal.* 177, 378 (**1998**).
25. Z. Huang, F. Cui, H. Kang, J. Chen, and C. Xia, *Appl. Catal. A: General* 366, 288 (**2009**).
26. Z. Huang, F. Cui, J. Xue, J. Zuo, J. Chen, and C. Xia, *Catal. Today* 183, 42 (**2012**).
27. P. Betancourt, A. Rives, R. Hubaut, C. E. Scott, and C. E. J. Goldwasser, *Appl. Catal. A: Gen.* 170, 307 (**1998**).
28. P. G. J. Koopman, A. P. G. Kieboom, and H. Van Bekkum, *J. Catal.* 69, 172 (**1981**).
29. D. E. Quesada, M. I. M. Ortiz, J. J. Jimenez, E. R. Castellon, and A. J. Lopez, *J. Mol. Catal. A: Chem.* 255, 41 (**2006**).
30. Y. Zheng, X. Chen, and Y. Shen, *Chem. Rev.* 108, 5253 (**2008**).
31. Q. Liu, X. Guo, Y. Li, and W. Shen, *Langmuir* 25, 6425 (**2009**).
32. R. D. Cortright, M. Sanchez-Castillo, and J. A. Dumesic, *Appl. Catal. B: Environ.* 39, 353 (**2002**).
33. Q. Liu, X. Guo, Y. Li, and W. Shen, *J. Phys. Chem. C.* 113, 3436 (**2009**).
34. Y. Nakagawa and K. Tomishige, *Catal. Sci. Technol.* 1, 179 (**2011**).
35. Y. Zheng, X. Chen, and Y. Shen, *Chem. Rev.* 108, 5253 (**2008**).
36. T. Miyazawa, Y. Kusunoki, K. Kunimori, and K. Tomishige, *J. Catal.* 240, 213 (**2006**).
37. C. H. C. Zhou, J. N. Beltramini, Y. X. Fan, and G. Q. M. Lu, *Chem. Soc. Rev.* 37, 527 (**2008**).

Received: 23 January 2013. Accepted: 14 March 2013.